Estimation of Shear-Banding Resistance in Metallic Glass Containing Nano-Crystalline Particles

Naoki Matsumoto [a], Ryosuke Matsumoto [b,*], and Noriyuki Miyazaki [b]

[a] *Graduate Student, Department of Mechanical Engineering and Science, Graduate School of Engineering, Kyoto University, Yoshida Honmachi, Sakyo-ku, Kyoto, 606-8501, Japan*

[b] *Department of Mechanical Engineering and Science, Graduate School of Engineering, Kyoto University, Yoshida Honmachi, Sakyo-ku, Kyoto, 606-8501, Japan*

Abstract

Bulk metallic glasses (BMGs) have a variety of excellent properties compared with the majority of conventional crystalline alloys. However, they exhibit limited global plasticity at room temperature because of shear banding. Several methods have been proposed to improve the limited ductility of BMG; one method is the homogeneous distribution of crystalline particles. However, our understanding of the interaction between the crystalline particles and shear bands (SB) is not sufficient. Here, we performed molecular dynamics (MD) simulations of mode II deformation of a notched BMG plate and BMG plates containing one nano-crystalline particle ahead of the notch bottom. To compare the effect of crystalline particle size on the resistance to SB propagation, we used the J-integral. By comparing J-R curves and the deformation behavior of the BMG plates with and without nano-crystalline particles, we found that the resistance to shear banding is efficiently improved by introducing crystalline

particles with sufficient size, compared to the SB width.

PACS: 62.20.F-; 64.70.pe; 62.25.Mn; 02.70.Ns

1. Introduction

Bulk metallic glasses (BMGs) have excellent properties [1, 2] such as a high elastic limit and good resistance to fatigue. However, due to shear banding, they exhibit limited global plasticity at room temperature. The shear bands (SB) in BMG are roughly planar and very thin (10–20 nm); they nucleate preferentially from surfaces, with intense heating and evidence of melting at the trailing edges [3, 4]. Recent research indicates that controlling the initiation and propagation of SBs is effective in enhancing the mechanical properties of BMG [5, 6]. Several methods have been proposed to improve the limited ductility of BMG [7-10], including homogeneous distribution of nano-sized crystalline particles. However, there has not been sufficient analysis of the interaction between crystalline particles and SBs. In particular, it is important to determine the most effective particle size and ideal crystal-volume fraction, because of difficulties in controlling the particle size and volume fraction and in experimental observation of internal structural changes.

Here we perform molecular dynamics (MD) simulations of mode II deformation of a notched $Zr_{65}Al_{7.5}Ni_{10}Cu_{17.5}$ BMG plate, and BMG plates containing one nano-crystalline particle of Ni ahead of the notch bottom. To compare the effect of the size of crystalline particles on SB propagation, we use the fracture-mechanical parameter J-integral. Comparing J-R curves, we investigate the appropriate size of crystalline particles for improving the ductility of BMGs.

2. Calculation method and simulation models

2.1. MD Simulation

Various properties of materials at an atomic level can be estimated through MD simulations by tracing the trajectories of all particles in a system. Experimental observation of atomic structural changes in amorphous structures is extremely difficult; therefore, MD simulations have been applied in many research studies [11-16]. In this study, we use the velocity-scaling method to control the temperature. The periodic boundary conditions are applied to the *x*, *y*, and *z*-axes in the generation process of the amorphous structure, and only to the *z*-axis in simulations of mode II deformation. We employed the generalized embedded-atom-method (GEAM) potential as an interatomic potential [17].

2.2. Preparation of BMG plates

An alloy plate with amorphous structure, which we call a BMG plate, was numerically produced by melting–rapid quenching MD simulations (see details in [12, 13]). The material composition was initially defined as $Zr_{65}Al_{7.5}Ni_{10}Cu_{17.5}$, and the thickness of plate L_z was determined as the periodic boundary condition applied to the thickness direction (*z*-axis) when a Ni nano-crystalline particle, whose [211] direction is taken in the *z*-axis, is introduced. The heating and quenching rate are both 1×10^{14} K/s. By this procedure, we obtained a BMG plate with a unit cell size (L_x, L_y, L_z) of about (82.8, 51.8, 2.16 nm), which is composed of about 500,000 atoms. We then introduced a notch of length L_c = 10 nm and bottom radius R_c = 2 nm at the center of the left edge, as shown in Fig. 1(a).

After generating the notched BMG plate, we introduced nano-crystalline

particles of various sizes into the BMG plate (see detail in [13]). Here, we chose $[0\bar{1}1]$ direction to the *x* direction, and this crystal orientation is the most deformable under the loading condition defined in the next section. The center of the particle was defined such that its left edge is placed at a distance of D = 15 nm from the notch bottom (Fig. 1(b)). We produced eight different models with particle diameters, d, of 3, 6, 9, 12, 15, 18, 21, and 24 nm, and labeled these A_3, A_6, A_9, A_{12}, A_{15}, A_{18}, A_{21}, and A_{24}, respectively. In addition, A_0 is the BMG plate without a crystalline particle.

2.3. Simulation conditions for Mode II deformation

In this study, the initial temperature of the notched plates was defined very low (1 K), to cause pronounced inhomogeneous deformations, or to enhance sharp SB nucleation and propagation. First, relaxation was performed for 10 ps under constant temperature, with the boundary atoms, which are located inside the cut-off distance (r_c = 0.648 nm) from the left, top, and bottom edges of the BMG plates, fixed in the *x*- and *y*-axis. After the relaxation, the upper half of the boundary atoms were moved to the right, and the lower half were moved to the left, with the displacement of all the boundary atoms controlled in the *y*-axis (Fig. 1(b)). In the initial 2 ps of deformation, the deformation velocity increased linearly until V = 50 m/s in order to reduce the propagation of elastic waves. No temperature control was applied during the shear-banding simulations.

2.4. Calculation of J-integral

We used the J-integral in the form of a domain integral. Equation (1) was employed for the J-integral to remove the influence of the distribution of initial stress and potential energy [12].

$$J = \sum_{\alpha \text{ in } S} \left[\left(\sigma_{ij}^{(\alpha)} - \sigma_{ij}^{0(\alpha)} \right) \frac{\partial u_i^{(\alpha)}}{\partial x_1} - \left(W^{(\alpha)} - W^{0(\alpha)} \right) \delta_{1j} \right] \frac{\partial Q}{\partial x_j} V^{(\alpha)} \frac{1}{L_z} \quad (1)$$

Here, $\sigma_{ij}^{(\alpha)}$ and $W^{(\alpha)}$ are the atomic stress tensor and the potential-energy density of atom α at the deformed state, and $\sigma_{ij}^{0(\alpha)}$ and $W^{0(\alpha)}$ are those at the initial state, respectively. $u_i^{(\alpha)}$ and $V^{(\alpha)}$ are the displacement and volume of atom α, and δ is Kronecker's delta. The integration domain S is constructed by the rectangular edges with a width of several nanometers surrounding the notch bottom (Fig. 1(b)), and Q is the linear function, whose value is 1 inside of the integral domain and 0 outside of the domain. In this study, we neglect the temperature effect on J, because the internal stress in BMGs is very high. Thus, the contribution of the temperature gradient is considered negligible.

3. Estimation of shear-banding resistance and discussions

3.1. Dependence of *J* on the integral domain

First, we calculated the J-integral for Model A_0 when the shear distance Δx is 8 nm, with changing width w_S and the distance from notch bottom to the right edge of the integral domain l_S (Fig. 2(a)), and then examined the influence of the integration domain. The dependence of J on the position of the right edge when the width of the integral domain w_S is 3 and 5 nm is shown in Fig. 2(b). The oscillation of the J-integral is large when the domain width is 3 nm; therefore, we need a wider integral domain. J becomes large when the distance from the notch bottom is longer than 60 nm; i.e., the distance between the right free edge and the right edge of the integration domain is shorter than about 10 nm. This is the influence of the free surface of the right edge of the BMG plate. From this result, we found that it is necessary to choose a distance between the notch bottom and the right edge of integral domain l_S less than 60 nm. Next,

we show J-displacement curves when the width of the integral domain is 5 and 7 nm (Fig. 2(c)). When the domain width is 5 nm, the oscillation of the J-integral due to the position of the right edge is large. On the other hand, when the width is 7 nm, the dispersion is comparatively small, and the J-integral becomes almost path independent. From these results, we choose w_S = 7 nm and l_S = 50 nm as the appropriate J-integral domain for the present models. The determined integration domain is shown in Fig. 1(a).

3.2. Dependence of shear-banding resistance on particle size

The J-displacement curves for a monolithic BMG plate (A_0) and BMG plates containing one crystalline particle (A_3, A_6, A_9, A_{12}, A_{15}, A_{18}, A_{21}, and A_{24}) are shown in Fig. 3(a). The values of the J-integral are considerably improved for the models containing crystalline particles with a diameter of more than 15 nm, compared to the values for A_0. Here, the horizontal axis of the J-R curves should be the crack extension Δa from the usual definition of the J-R curves that are used to estimate ductile crack growth behavior. Crack growth is not always observed for BMG, and the propagation of SB is considered more essential. In this study, we used the extension of a high-temperature region that appears in SBs as the definition of Δa, because the higher the temperature, the lower the resistance to deformations, thus making the resistance very small. We employed T_c = 350 K as the critical temperature. Thus, the x-component of the distance between the notch bottom and the leading edge of the region over 350 K is defined as Δa (Fig. 3 (b)). Figure 3 (c) shows the relationship between Δx and Δa for model A_0. Finally, we changed the horizontal axis of the J-displacement curves from Δx to Δa and obtained the J-R curves (Fig. 3 (d)). We also show the slopes of the R curves dJ/da, and the slopes of the lines of the second stage of the J-R curves (Fig. 3(e)). The

slopes represent stability of SB growth. When a crystalline particle with a diameter larger than 15 nm is introduced, the slope becomes steeper. This result indicates that these larger crystalline particles improve the shear-banding resistance of BMGs in this simulation condition.

In this study, we chose T_c = 350 K for the critical temperature because of the limitation of time and spatial scales of the MD simulations; this temperature is considerably lower than the glass transition temperature T_g. However, we believe that the influence of T_c on the particle-size effect is very small, because Δa increases almost linearly in Fig. 2 (c); therefore, the change in T_c only alters the turnoff point of the J-R curves J_c and a small part of the slope of dJ/da.

3.3. Relationship between the J-integral and the deformation state

To investigate the relationship between the J-R curve and deformation state, we evaluated the distributions of the equivalent strain using the weighted function [14]. The distributions for A_0, A_6, and A_{15} at Δx = 16 nm are shown in Fig. 4. Since the crystalline particles are very small and they include no defects, the crystalline particles are harder than the amorphous phase. Despite the most deformable crystal orientation, they do not undergo deformation. When the crystalline particle is small, as in A_6, the particle is swallowed by the primary SB developed from the notch bottom (Fig. 4 (b)). Introducing a crystalline particle with a diameter of 15 nm, however, notably changes the shape of the region with high equivalent strain (Fig. 4 (c)). The boundary particle size (~15 nm) is close to the width of the primary SB in BMG without a crystalline particle (A_0) (Fig. 4 (a)). Consequently, we consider that a crystalline particle of sufficient size, compared to the width of SBs at the position of the particle, is necessary to prevent the propagation of the SB or to change the propagation path.

On the other hand, hard nano-crystalline particles can also work as a nucleation source of SBs [15]. In this calculation, we can also observe the nucleation of SBs around the crystalline particle (arrows in Fig. 4(c)). Since the effect of particle size on the nucleation of SBs is quite small [15], the increase in particle size leads to a decrease in the density of the deformation source under the same crystal-volume fraction, and therefore, the plastic work around the primary SB is reduced. Moreover, for coarse arrangements of crystalline particles, the primary SB can grow more easily up to the critical length, which potentially causes catastrophic propagation [16]. It is considered that once the unstable SBs are generated, the growth of the SBs cannot stop without the use of some mechanism capable of arresting running SB such as soft inhomogeneities. Therefore we consider that, for the introduction of hard crystalline particles, an appropriate particle size for efficiently improving the ductility exists.

4. Conclusion

By estimating the dependence of J on the integral domain, we employed the reliable domain. Further, by evaluating J-R curves, we found that the shear-banding resistance of BMG is improved by introducing crystalline particles with a sufficient size, compared to the width of the SB. On the other hand, an increase in particle size leads to a decrease in the nucleation source of SBs. Therefore, we find that an appropriate particle size that provides the best ductility exists.

Acknowledgements

This research was supported by the Ministry of Education, Culture, Sports, Science and Technology of Japan, Grant-in-Aid for Scientific Research on Priority

Areas, “Materials Sciences of Bulk Metallic Glasses.”

Reference

[1] A. Inoue, Acta Materialia, 48 (2000) pp. 279-306.

[2] A. L. Greer, Science, 267 (1995) pp. 1947-1953.

[3] J. J. Lewandowski, A. L. Greer, Nature Materials, 5 (2006) pp. 15-18.

[4] B. Yang, M. L. Morrison, P. K. Liaw, R. A. Buchanan, G. Wang, C. T. Liu, M. Denda, Applied Physics Letters, 86 (2005) 141904.

[5] C. A. Schuh, T. C. Hufnagel, U. Ramamurty, Acta Materialia, 55 (2007) pp. 4067-4109.

[6] A. V. Sergueeva, N. A. Mara, J. D. Kuntz, D. J. Branagan, A. K. Mukherjee, Materials Science and Engineering A, 383 (2004) pp. 219-223.

[7] X. Y. Jiang, Z. C. Zhong, A. L. Greer, Materials Science and Engineering A, 226-228 (1997) pp. 789-793.

[8] Y. H. Kim, A. Inoue, T. Masumoto, Materials Transactions JIM, 32-7 (1991) pp. 599-608.

[9] B. Cantor, *Novel Nanocrystalline Alloys and Magnetic Nanomaterials*, Institute of Physics, 2005.

[10] D.C. Hofmann, J.-Y. Suh, A. Wiest, G. Duan, M.-L. Lind, M.D. Demetriou and W.L. Johnson, Nature, 451 (2008) pp. 1085-1089.

[11] F. Shimizu, S. Ogata, J. Li, Acta Materialia, 54 (2006) pp. 4293-4298.

[12] K. Nakatani, A. Nakatani, Y. Sugiyama, H. Kitagawa, AIAA Journal, 38-4 (2000) pp. 695-701.

[13] R. Matsumoto, M. Nakagaki, Modelling Simulation in Materials Science and Engineering, 14 (2006) pp. S47-S54.

[14] R. Matsumoto, M. Nakagaki, CMES: Computer Modeling in Engineering and Science, 10 (2005) pp. 187-197.

[15] J. Park, Y. Shibutani, M. Wakeda, S. Ogata, Materials Transaction, 48 (2007) pp. 1001-1006.

[16] R. Matsumoto, N. Miyazaki, Scripta Materialia, 59 (2008) pp. 107-110.

[17] X. W. Zhou, R. A. Johnson, H. N. G. Wadley, Physical Review B 69 (2004) 144113.

Figure captions

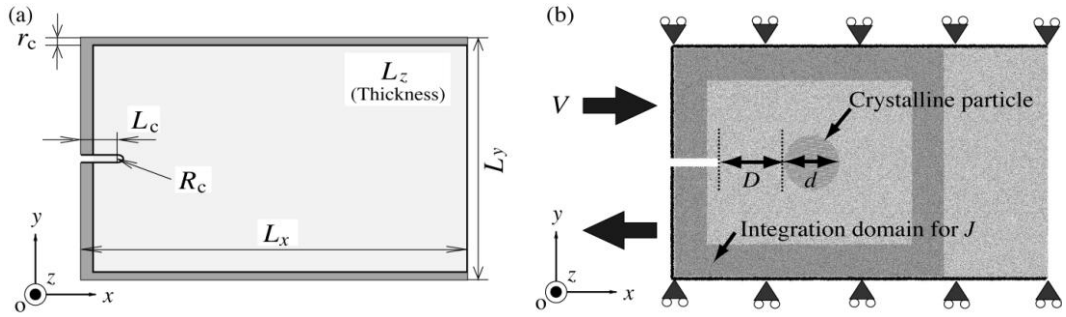

Figure 1: Simulation model: (a) Geometry of the simulation model. (b) Boundary conditions, position of the crystalline particle, and appropriate integral domain for the J-integral. The left edge of the particle is placed at a distance of D = 15 nm to the right of the notch bottom. The diameter of the particle in this figure is d = 12 nm.

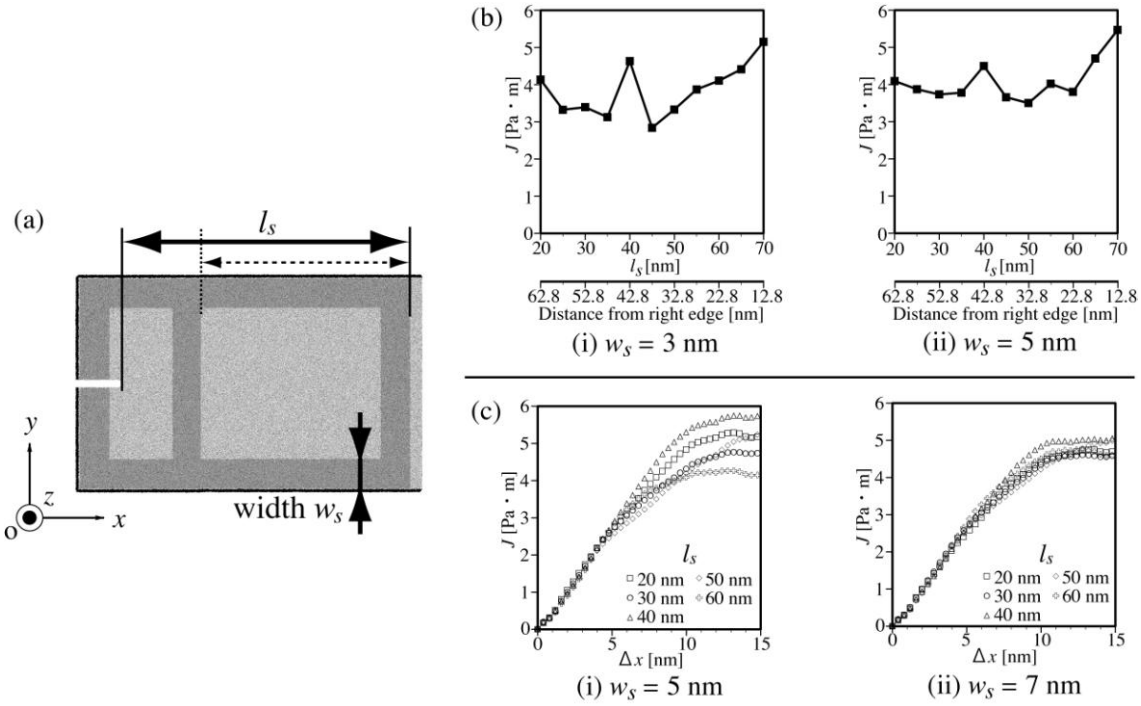

Figure 2: Dependence of J on the integral domain: (a) Definition of the width of integral domain w_S and distance from the notch bottom to the right edge of the integral domain l_S. l_S is changed by moving the right region of the integral domain, as shown by the dotted arrow. (b) Dependence of J on the position of the right edge of integral domain (Δx = 8 nm). (c) Influence of w_S and l_S on the J-displacement curve.

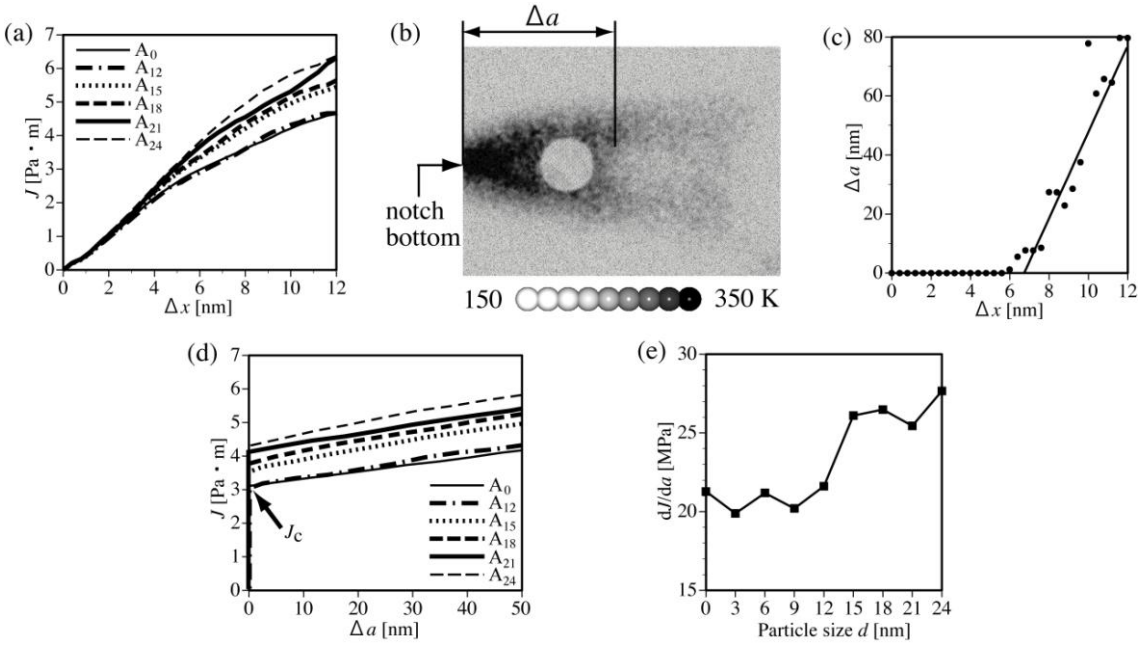

Figure 3: J-integral and J-R curves: (a) J-displacement curves. (b) Definition of SB extension Δa. The critical temperature was chosen as T_c = 350 K. (c) Relationship between shear displacement Δx and SB extension Δa for A_0. (d) J-R curves converted from J-displacement curves, using the relationship between Δx and Δa. (e) Dependence of the slope of the R curves dJ/da on particle size.

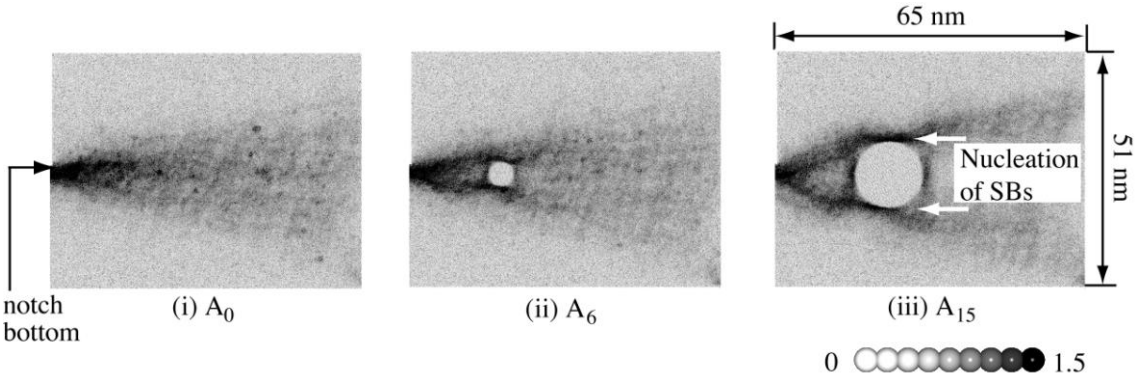

Figure 4: Distribution of equivalent strain (Δx = 16 nm).